LETTERS

Impaired hippocampal–prefrontal synchrony in a genetic mouse model of schizophrenia

Torfi Sigurdsson[1], Kimberly L. Stark[1,2], Maria Karayiorgou[1,4], Joseph A. Gogos[2,3] & Joshua A. Gordon[1,4]

Abnormalities in functional connectivity between brain areas have been postulated as an important pathophysiological mechanism underlying schizophrenia[1,2]. In particular, macroscopic measurements of brain activity in patients suggest that functional connectivity between the frontal and temporal lobes may be altered[3,4]. However, it remains unclear whether such dysconnectivity relates to the aetiology of the illness, and how it is manifested in the activity of neural circuits. Because schizophrenia has a strong genetic component[5], animal models of genetic risk factors are likely to aid our understanding of the pathogenesis and pathophysiology of the disease. Here we study *Df(16)A*$^{+/-}$ mice, which model a microdeletion on human chromosome 22 (22q11.2) that constitutes one of the largest known genetic risk factors for schizophrenia[6]. To examine functional connectivity in these mice, we measured the synchronization of neural activity between the hippocampus and the prefrontal cortex during the performance of a task requiring working memory, which is one of the cognitive functions disrupted in the disease. In wild-type mice, hippocampal–prefrontal synchrony increased during working memory performance, consistent with previous reports in rats[7]. *Df(16)A*$^{+/-}$ mice, which are impaired in the acquisition of the task, showed drastically reduced synchrony, measured both by phase-locking of prefrontal cells to hippocampal theta oscillations and by coherence of prefrontal and hippocampal local field potentials. Furthermore, the magnitude of hippocampal–prefrontal coherence at the onset of training could be used to predict the time it took the *Df(16)A*$^{+/-}$ mice to learn the task and increased more slowly during task acquisition. These data suggest how the deficits in functional connectivity observed in patients with schizophrenia may be realized at the single-neuron level. Our findings further suggest that impaired long-range synchrony of neural activity is one consequence of the 22q11.2 deletion and may be a fundamental component of the pathophysiology underlying schizophrenia.

Despite decades of research, the neural circuit abnormalities underlying schizophrenia remain elusive. Abnormal long-range connectivity between brain areas was proposed as a potential pathophysiological mechanism more than 100 years ago[1,2]. In support of this hypothesis, recent neuroimaging[3,4] and electroencephalographic[8] studies suggest that functional connectivity between the prefrontal cortex and the temporal lobe, including the hippocampus, is abnormal in schizophrenia patients. However, it remains unclear how such findings relate to aetiological factors, such as genetic risk variants. Moreover, the macroscopic measurements of brain activity used in patient studies cannot address how abnormal connectivity is manifested within neural circuits, which is a crucial step if the pathophysiology of schizophrenia is to be understood in detail. Mouse models of schizophrenia predisposition are likely to be important in clarifying these issues, because they make it possible to directly assess the impact of schizophrenia risk alleles on neural activity across multiple brain areas.

One unequivocal risk allele is the 22q11.2 microdeletion, which increases the risk of developing schizophrenia ~30-fold[9–12]. We have recently engineered and characterized a line of mice (*Df(16)A*$^{+/-}$) with a microdeletion in the region of chromosome 16 syntenic to the core 1.5-megabase microdeletion found in patients with schizophrenia[13,14]. *Df(16)A*$^{+/-}$ mice have several abnormalities analogous to those seen in individuals with schizophrenia, notably working memory impairments. Such impairments, although not part of the diagnostic criteria for schizophrenia, are nonetheless core features of the illness. They are probably mediated by the same genetic risk factors and abnormal physiological processes[15], and are more amenable to study in animal models than are other symptoms such as psychosis. In rats, neural activity in the hippocampus and prefrontal cortex becomes synchronized during the performance of a spatial working memory task[7]; lesion studies suggest that such interactions are necessary for successful task performance[16]. Studying whether hippocampal–prefrontal synchrony is disrupted in an animal model of an unequivocal causal factor of schizophrenia would be of considerable value in furthering our understanding of the pathophysiology of the disorder.

To verify that spatial working memory in mice involves hippocampal–prefrontal synchrony, we recorded neural activity simultaneously in the hippocampus and medial prefrontal cortex of wild-type C57BL/6J mice while they performed a discrete-trial T-maze task (Fig. 1a). Each trial of the task comprised a 'sample phase', in which animals were directed to enter one of two goal arms, and a 'choice phase', in which animals had to remember the arm visited during the sample phase and enter the opposite arm (Fig. 1a). Robust hippocampal–prefrontal synchrony was observed during this task using two independent measures: the modulation of prefrontal neuron spiking by hippocampal theta-frequency (4–12-Hz) oscillations (phase-locking; Fig. 1b–e), and the coherence of prefrontal and hippocampal local field potentials in the theta frequency range (theta coherence; Fig. 1h). Prefrontal neurons tended to phase-lock most strongly to the peak of the hippocampal theta oscillation of the recent past (Fig. 1e, f), suggesting that hippocampal afferents drive prefrontal activity[7,17]. Significantly, hippocampal–prefrontal synchrony was modulated by the mnemonic demands of the task: both phase-locking ($P = 0.031$, Wilcoxon signed-rank test, $n = 65$ neurons; Fig. 1g) and theta coherence ($P = 0.019$, paired t-test of 4–12-Hz coherence, $n = 9$ animals; Fig. 1h) were significantly stronger in the choice phase, which requires working memory, than in the sample phase, which does not. In contrast, neither phase-locking nor coherence in the delta range (1–4 Hz) or the gamma range (30–80 Hz) increased in the choice phase ($P > 0.05$; data not shown). These data demonstrate that in the mouse, as in the rat[7], theta-frequency synchrony marks the functional

[1]Department of Psychiatry, [2]Department of Physiology and Cellular Biophysics, [3]Department of Neuroscience, College of Physicians and Surgeons, Columbia University, New York, New York 10032, USA. [4]New York State Psychiatric Institute, New York, New York 10032, USA.

©2010 Macmillan Publishers Limited. All rights reserved

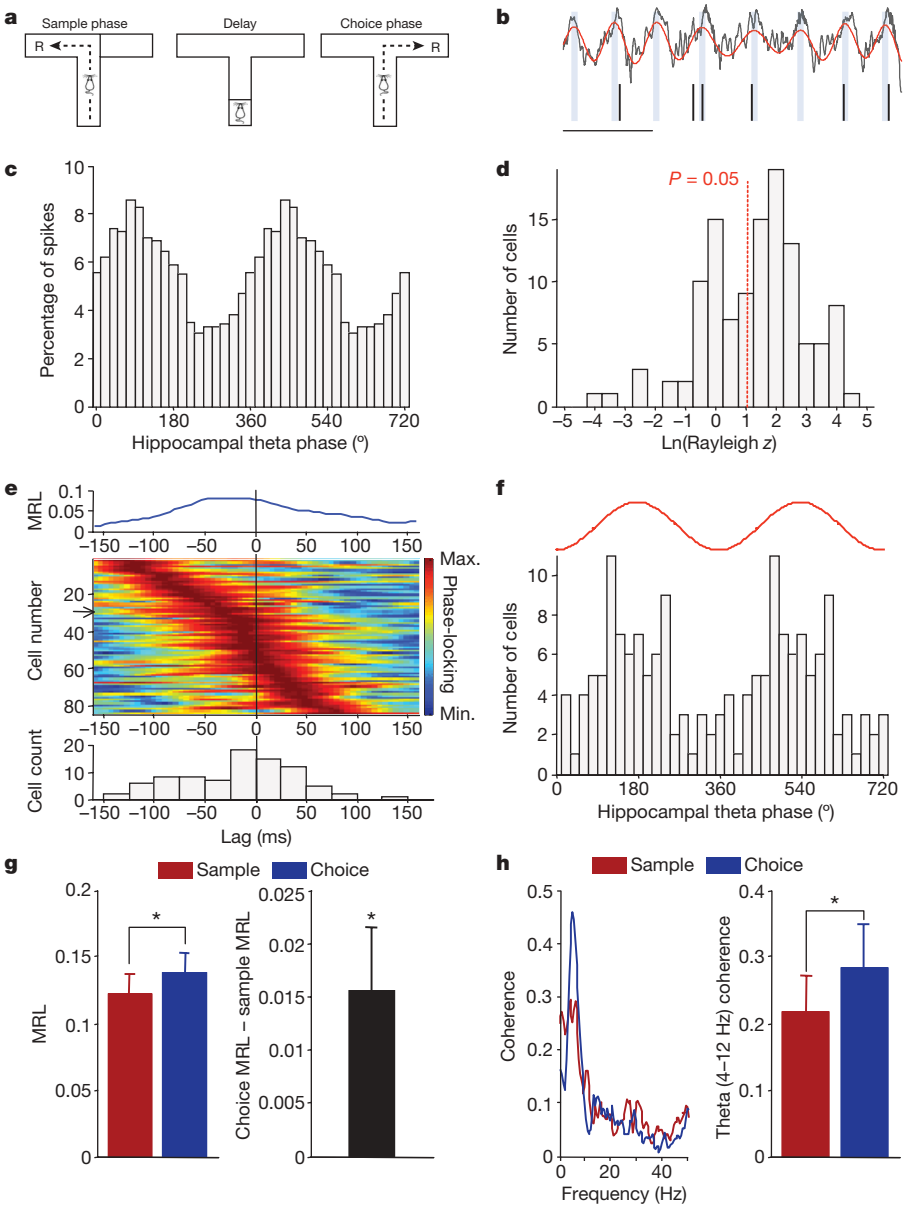

Figure 1 | Hippocampal–prefrontal synchrony during a spatial working memory task in mice. **a**, Spatial working memory task (see text). R, reward. **b**, Example field potential recording from the hippocampus (black trace) showing theta oscillations (red trace) and spikes recorded simultaneously from a prefrontal neuron (tick marks). Scale bar, 200 ms. **c**, Distribution of hippocampal theta phases at which the neuron in **b** fired. **d**, Distribution of Rayleigh *z* scores, for estimating significance of phase-locking to hippocampal theta oscillations, for prefrontal neurons recorded from wild-type mice. The red line denotes the significance threshold ($P < 0.05$); 83 of 125 neurons were significantly phase-locked. **e**, Prefrontal neurons phase-lock most strongly to the theta phase of the past. Top: strength of phase-locking of a single prefrontal neuron as a function of lag between the prefrontal spike and the hippocampal field potential recording. MRL, mean resultant length (Methods). Middle: normalized phase-locking strength of each neuron as a function of lag. Rows represent individual neurons ordered by the lag of maximal phase-locking. Arrow, neuron corresponding to trace at top. Bottom: distribution of lags at which each cell was maximally phase-locked (lag, -17.5 ± 6.2 ms (mean ± s.e.m.); $P = 0.016$; Wilcoxon signed-rank test). **f**, Distribution of hippocampal theta phases to which prefrontal neurons are significantly phase-locked (mean ± 95% confidence interval, $166^\circ \pm 43.8^\circ$; $P = 0.0005$, Rayleigh test). The red trace is a schematic of a single theta cycle. **g**, Phase-locking strength in the centre arm of the maze during sample and choice phases (left) and the difference in phase-locking across the two conditions (right). **h**, Coherence between hippocampal and prefrontal field potentials during the same task phases as in **g**: an example of coherence in one session (left); theta coherence (4–12 Hz) across animals (right). *$P < 0.05$; data shown, mean ± s.e.m.

connectivity between the hippocampus and the prefrontal cortex that is required for proper spatial working memory function.

We next examined hippocampal–prefrontal synchrony in *Df(16)A*$^{+/-}$ mice and their wild-type littermates as they performed the same T-maze task. To ensure that differences in task performance would not influence the results, mice of both genotypes were trained to equal levels of choice accuracy (Supplementary Fig. 1c; see also Supplementary Table 1). Neurons recorded from the prefrontal cortex of *Df(16)A*$^{+/-}$ mice ($n = 88$) did not differ from neurons recorded from wild-type mice in basic firing properties or isolation quality (Supplementary Fig. 2). Furthermore, many neurons (51 of 88, $P < 0.05$, Rayleigh test) recorded from *Df(16)A*$^{+/-}$ mice displayed significant phase-locking to the hippocampal theta rhythm that was qualitatively similar to that in wild-type mice (Supplementary Fig. 3). However, the strength of phase-locking was considerably lower in *Df(16)A*$^{+/-}$ mice than in wild-type mice ($P = 0.004$, Wilcoxon rank-sum test, $n = 94$ neurons from wild-type mice and 81 neurons from *Df(16)A*$^{+/-}$ mice; Fig. 2a), suggesting a deficit in theta-frequency synchrony.

We next determined whether the phase-locking deficit in the *Df(16)A*$^{+/-}$ mice was modulated by the mnemonic demands of the

©2010 Macmillan Publishers Limited. All rights reserved

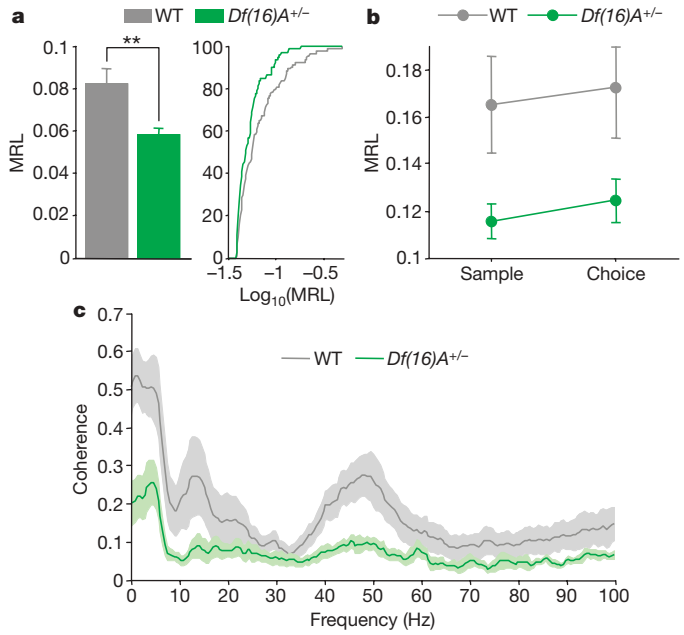

Figure 2 | Reduced hippocampal–prefrontal synchrony in *Df(16)A*$^{+/-}$ mice. **a**, Phase-locking of prefrontal neurons to hippocampal theta (left) and cumulative distribution of phase-locking values (right) in the two genotypes. Phase-locking is stronger in wild-type mice. $^{**}P < 0.01$; WT, wild type. **b**, Phase-locking strength in the centre arm during sample and choice phases. **c**, Coherence between hippocampal and prefrontal field potentials during the choice phase as in **b**. Coherence is lower in *Df(16)A*$^{+/-}$ mice. Data shown, mean ± s.e.m.

task. As before, we restricted our analysis to neural activity recorded in the centre arm during sample and choice phases. This had the advantage of minimizing behavioural variability, as both the trajectories and the speeds of centre-arm runs were comparable between genotypes (Supplementary Fig. 1a, b). As shown in Fig. 2b, phase-locking was stronger in neurons from wild-type mice than from *Df(16)A*$^{+/-}$ mice during both task phases, although *Df(16)A*$^{+/-}$ neurons displayed a comparable increase in the strength of phase-locking during the choice phase. This was confirmed in a two-way analysis of variance (task phase by genotype) that revealed a main effect of genotype ($F_{1,\ 87} = 5.72$, $P = 0.019$) and task phase ($F_{1,\ 87} = 6.43$, $P = 0.013$) but no significant interaction ($F_{1,\ 87} = 0.22$, $P = 0.64$). Differences in synchrony were also evident in the coherence of hippocampal and prefrontal field potentials, which was lower in *Df(16)A*$^{+/-}$ mice than in wild-type littermates across multiple frequency ranges (Fig. 2c). A two-way analysis of variance revealed a significant genotype by frequency interaction ($F_{211,\ 2,321} = 3.14$, $P < 0.0001$), and coherence was significantly lower in *Df(16)A*$^{+/-}$ mice than in wild-type mice at frequencies in the delta range (1–4 Hz) and the low theta range (4–6 Hz) ($P < 0.05$, Bonferroni tests). Coherence differences at higher theta frequencies (7–10 Hz) and in the gamma range (30–80 Hz) were not statistically significant after correction for multiple comparisons.

Consistent with our previous finding[14], *Df(16)A*$^{+/-}$ mice required more training than did wild-type mice to reach criterion (three consecutive days during which at least 70% of all choices are correct; Fig. 3b), although this effect did not reach statistical significance ($P = 0.13$, unpaired *t*-test), probably owing to differences in sample size between studies ($n = 9$ or 10 per genotype in the present study and $n = 20$ in ref. 14). A learning impairment raises the possibility that differences in synchrony could result from learning-related changes in this circuit emerging differentially in the two genotypes, particularly if the mice were to use different strategies to solve the task. To address this issue, we asked whether deficits in synchrony existed before training, by analysing data from centre-arm runs during habituation sessions. We used coherence to measure synchrony because too few single units were recorded before training to obtain reliable measures of phase-locking. Coherence was lower in the *Df(16)A*$^{+/-}$ mice than in wild-type mice before training (Fig. 3a), as shown by a highly significant genotype by frequency interaction (repeated-measure analysis of variance, $F_{211,\ 3,587} = 2.12$, $P < 0.0001$), suggesting that impaired synchrony is a baseline property of the hippocampal–prefrontal circuit in *Df(16)A*$^{+/-}$ mice. Coherence differences were statistically significant within the delta range (2–3 Hz, $P < 0.05$, Bonferroni tests). Differences in the theta and gamma ranges were not statistically significant after correction for multiple comparisons.

To test whether these deficits in synchrony might contribute to the working memory impairments in *Df(16)A*$^{+/-}$ mice, we examined

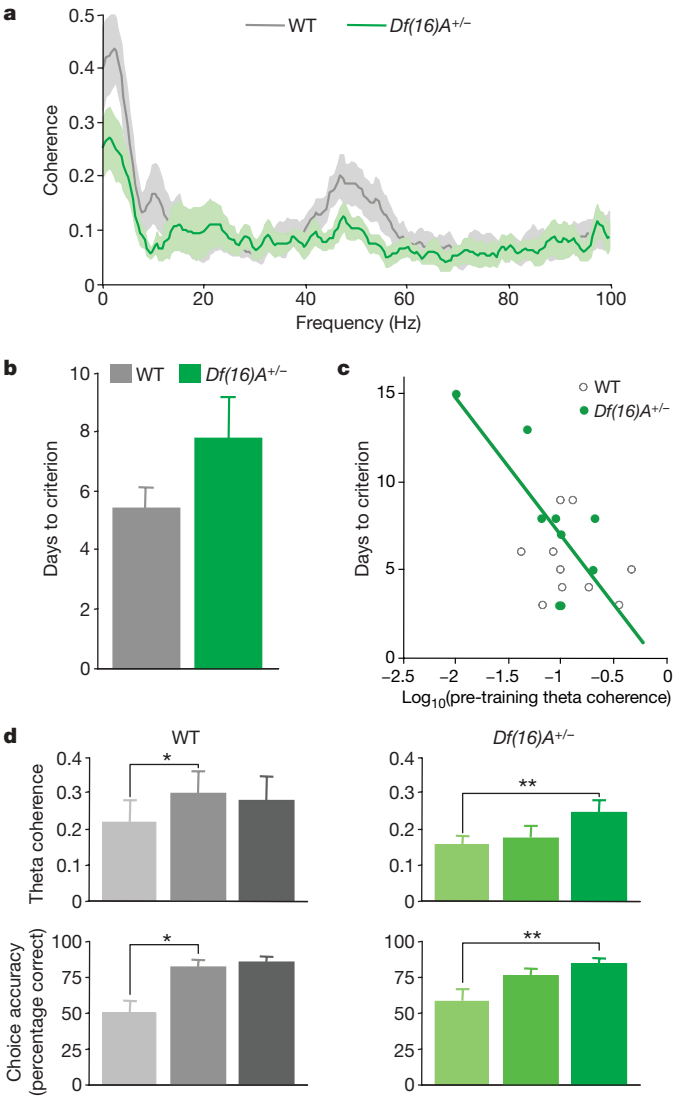

Figure 3 | Reduced hippocampal–prefrontal synchrony correlates with behavioural performance in *Df(16)A*$^{+/-}$ mice. **a**, Coherence between the prefrontal cortex and the hippocampus during habituation sessions before training on the spatial working memory task. **b**, Days taken to reach criterion performance on the spatial working memory task. **c**, Days taken to reach criterion versus theta coherence during habituation sessions for each animal. Animals with lower theta coherence before training take longer to learn the spatial working memory task. Green line, linear regression of data from *Df(16)A*$^{+/-}$ mice. **d**, Development of hippocampal–prefrontal coherence during acquisition of the working memory task: theta coherence (top) and choice accuracy (bottom) during early (trials 1–5), middle (trials 26–30) and late (session in which criterion was reached) stages of training in wild-type (left) and *Df(16)A*$^{+/-}$ (right) mice. $^{*}P < 0.05$, $^{**}P < 0.01$. Data shown, mean ± s.e.m.

©2010 Macmillan Publishers Limited. All rights reserved

whether theta coherence before training could be used to predict the subsequent learning rate in the T-maze, and how theta coherence developed during training. Theta coherence was used as a measure of synchrony because of its unequivocal association with working-memory-dependent behaviour[7] (Fig. 1h). As shown in Fig. 3c, animals with stronger theta coherence before training took fewer days to reach criterion (genotype-by-coherence analysis of covariance, $P = 0.0097$ for a main effect of coherence). This relationship could also be observed in the *Df(16)A*$^{+/-}$ mice alone (correlation coefficient, $r = -0.75$; $P = 0.02$) but did not reach significance in wild-type mice ($P = 0.49$). Similar results were obtained using a different learning criterion that is also used in the literature (two consecutive days during which at least 70% of all choices are correct; see Supplementary Fig. 4). During training, hippocampal–prefrontal synchrony increased in parallel with performance in both genotypes (Fig. 3d). In wild-type mice, both theta coherence ($P = 0.012$, paired *t*-test) and choice accuracy ($P = 0.005$) improved between early (trials 1–5) and middle (trials 26–30) phases of training. In contrast, neither theta coherence ($P = 0.26$) nor choice accuracy ($P = 0.086$) changed between early and middle training phases in *Df(16)A*$^{+/-}$ mice, but both increased in the late phase (when animals reached criterion performance; $P = 0.0008$ and 0.016 for coherence and behaviour, respectively). These effects were not dependent on the specific definition of trial phases (Supplementary Fig. 5). These results suggest that an increase in hippocampal–prefrontal synchrony during learning enables animals to acquire the working memory task successfully. Furthermore, the delayed increase in *Df(16)A*$^{+/-}$ mice, taken together with the finding that pre-training coherence predicts their learning rate, suggests that diminished hippocampal–prefrontal synchrony contributes to their working memory impairments.

Our data suggest that synchrony between the hippocampus and prefrontal cortex is reduced in the *Df(16)A*$^{+/-}$ mice relative to wild-type mice, but it is possible that this could be a consequence of impaired synchrony within these regions. Several observations argue against this possibility. First, although prefrontal neurons from *Df(16)A*$^{+/-}$ mice showed diminished phase-locking to the hippocampal theta rhythm, their phase-locking to the prefrontal theta rhythm was unaffected ($P = 0.30$, Wilcoxon rank-sum test, *n* values as in Fig. 2a; Fig. 4a) and the magnitude of the local prefrontal theta rhythm was unchanged ($P = 0.30$, *t*-test comparing 4–12-Hz power; Fig. 4b). Second, the reduction in phase-locking to the hippocampal theta rhythm was not the result of an impaired hippocampal theta rhythm, because its magnitude did not differ by genotype ($P = 0.30$, analysis as in Fig. 4b; Fig. 4c), and no qualitative or quantitative differences in theta oscillations were seen (Supplementary Fig. 6). Finally, we examined intrahippocampal synchrony by measuring the modulation of hippocampal gamma power by hippocampal theta phase[18] (Methods). This yielded modulation indices that were comparable between the two genotypes ($P = 0.71$, *t*-test; Fig. 4d), suggesting that the hippocampal theta oscillations are sufficiently capable of organizing activity within the hippocampus in *Df(16)A*$^{+/-}$ mice.

Our results demonstrate that a mutation associated with high risk for schizophrenia—the 22q11.2 microdeletion—disrupts synchrony between the hippocampus and prefrontal cortex. Both phase-locking of prefrontal neurons to hippocampal theta oscillations and coherence of prefrontal and hippocampal local field potentials were reduced in a mouse model of the 22q11.2 microdeletion, relative to wild-type mice. Our results further suggest that this reduced synchrony contributes to the working memory deficits observed in these mice. Notably, in addition to being a strong predisposing factor for schizophrenia in humans, the 22q11.2 deletion is associated with cognitive deficits, including working memory impairments[19,20]. These deficits are observed even in premorbid children and adolescent 22q11.2 carriers[21] and are associated with reduced frontal lobe activation[19]. Thus, the 22q11.2 deletion may contribute to the development of schizophrenia by altering prefrontal function and connectivity. Indeed, abnormal coupling has been observed between the prefrontal cortex and regions of the temporal lobe, including the hippocampus, both in schizophrenia patients[3,4,8] and in healthy individuals carrying candidate risk variants[22,23]. Our findings extend beyond patient studies by showing how disrupted connectivity can arise at the level of single neurons, as a result of an unequivocal genetic risk variant. Hippocampal–prefrontal synchrony is probably mediated through anatomical connections, both direct and indirect, between these two structures. An important

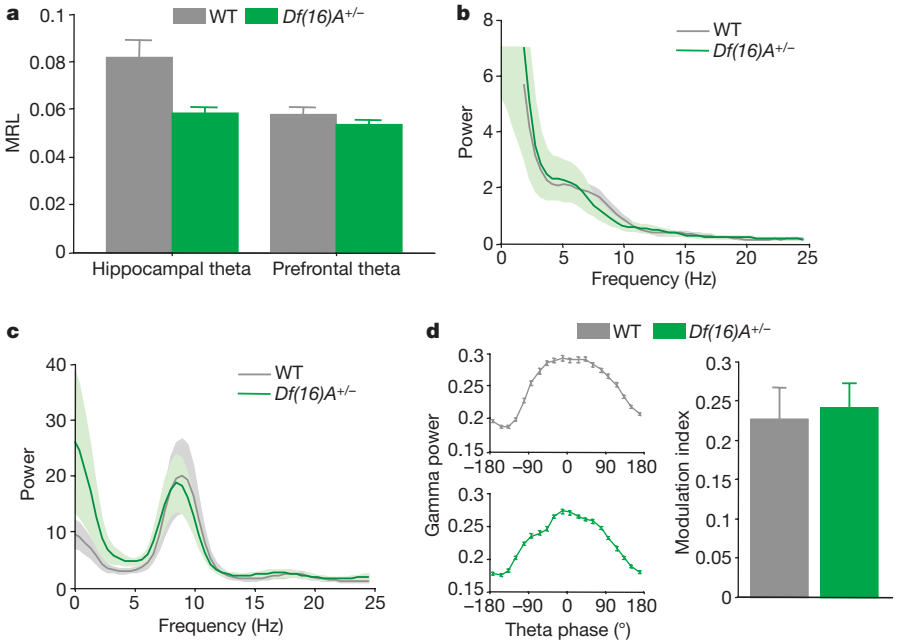

Figure 4 | Selectivity of hippocampal–prefrontal synchrony deficits in *Df(16)A*$^{+/-}$ mice. **a**, Comparison of phase-locking to theta oscillations in prefrontal cortex and hippocampus across the two genotypes. Phase-locking to prefrontal theta oscillations is intact. **b**, **c**, Field potential power in the prefrontal cortex (**b**) and hippocampus (**c**). **d**, Modulation of hippocampal gamma (30–80-Hz) power by theta phase. Left: examples of theta–gamma modulation in a wild-type mouse (top) and in a *Df(16)A*$^{+/-}$ mouse (bottom). Right: mean theta–gamma modulation index (Methods). Data shown, mean ± s.e.m.

©2010 Macmillan Publishers Limited. All rights reserved

next step will therefore be to examine the morphological and synaptic properties of these connections in *Df(16)A*$^{+/-}$ mice. Future experiments will further investigate how individual or cumulative contributions of genes affected by the 22q11.2 microdeletion[13,14,24–28] affect inter-areal synchrony in the brain[22], and will thus help reveal the mechanisms underlying its disruption in schizophrenia.

METHODS SUMMARY

We generated *Df(16)A*$^{+/-}$ mice and their wild-type littermates on a pure (>99.9%) C57BL/6J background (The Jackson Laboratory) as previously described[13,14]. All mice were 3–6 months old at the time of the experiments. Animals were implanted with recording electrodes in the medial prefrontal cortex and the dorsal CA1 region of the hippocampus (Supplementary Fig. 7). After they had recovered from surgery for a week, we put the animals on a restricted diet until their weight reached 85% of their pre-surgical weight. They were then trained on a discrete non-match-to-sample spatial working memory task in a T-maze, until they reached criterion performance. During performance of the task, neural data (putative spikes and field potentials) were acquired using a 16-channel headstage and a Cheetah32 data acquisition system (Neuralynx). Each animal's position in the maze was monitored using two light-emitting diodes mounted on the headstage. To extract putative spikes, neural signals were band-pass-filtered between 0.6 and 6 kHz and waveforms that passed a threshold were digitized at 30 kHz. Waveforms were then sorted into single-unit clusters using SPIKESORT3D (version 2.3, Neuralynx). To extract field potential activity, the same signals were band-pass-filtered between 1 and 1,000 Hz and digitized at 2 kHz. Further analysis of neural and behavioural data was performed using custom written MATLAB (version 7.6, MathWorks) scripts. We measured synchrony between hippocampal and prefrontal neural activity using two approaches. First, we examined the degree to which the firing of prefrontal neurons was modulated by the phase of the theta oscillation in the hippocampus. Second, we quantified the coherence between field potentials recorded in the two structures. All procedures were conducted in accordance with US National Institutes of Health regulations and approved by the Columbia University and New York State Psychiatric Institute Institutional Animal Care and Use Committees.

Full Methods and any associated references are available in the online version of the paper at www.nature.com/nature.

Received 6 May 2009; accepted 14 January 2010.

1. Stephan, K. E., Friston, K. J. & Frith, C. D. Dysconnection in schizophrenia: from abnormal synaptic plasticity to failures of self-monitoring. *Schizophr. Bull.* **35,** 509–527 (2009).
2. Wernicke, C. *Grundrisse der Psychiatrie* (Thieme, 1906).
3. Meyer-Lindenberg, A. S. *et al.* Regionally specific disturbance of dorsolateral prefrontal-hippocampal functional connectivity in schizophrenia. *Arch. Gen. Psychiatry* **62,** 379–386 (2005).
4. Lawrie, S. M. *et al.* Reduced frontotemporal functional connectivity in schizophrenia associated with auditory hallucinations. *Biol. Psychiatry* **51,** 1008–1011 (2002).
5. Gottesman, I. I. & Shields, J. A polygenic theory of schizophrenia. *Proc. Natl Acad. Sci. USA* **58,** 199–205 (1967).
6. Karayiorgou, M. & Gogos, J. A. The molecular genetics of the 22q11-associated schizophrenia. *Brain Res. Mol. Brain Res.* **132,** 95–104 (2004).
7. Jones, M. W. & Wilson, M. A. Theta rhythms coordinate hippocampal-prefrontal interactions in a spatial memory task. *PLoS Biol.* **3,** e402 (2005).
8. Ford, J. M., Mathalon, D. H., Whitfield, S., Faustman, W. O. & Roth, W. T. Reduced communication between frontal and temporal lobes during talking in schizophrenia. *Biol. Psychiatry* **51,** 485–492 (2002).
9. Karayiorgou, M. *et al.* Schizophrenia susceptibility associated with interstitial deletions of chromosome 22q11. *Proc. Natl Acad. Sci. USA* **92,** 7612–7616 (1995).
10. Xu, B. *et al.* Strong association of *de novo* copy number mutations with sporadic schizophrenia. *Nature Genet.* **40,** 880–885 (2008).
11. The International Schizophrenia Consortium. Rare chromosomal deletions and duplications increase risk of schizophrenia. *Nature* **455,** 237–241 (2008).
12. Stefansson, H. *et al.* Large recurrent microdeletions associated with schizophrenia. *Nature* **455,** 232–236 (2008).
13. Mukai, J. *et al.* Palmitoylation-dependent neurodevelopmental deficits in a mouse model of 22q11 microdeletion. *Nature Neurosci.* **11,** 1302–1310 (2008).
14. Stark, K. L. *et al.* Altered brain microRNA biogenesis contributes to phenotypic deficits in a 22q11-deletion mouse model. *Nature Genet.* **40,** 751–760 (2008).
15. Forbes, N. F., Carrick, L. A., McIntosh, A. M. & Lawrie, S. M. Working memory in schizophrenia: a meta-analysis. *Psychol. Med.* **39,** 889–905 (2009).
16. Floresco, S. B., Seamans, J. K. & Phillips, A. G. Selective roles for hippocampal, prefrontal cortical, and ventral striatal circuits in radial-arm maze tasks with or without a delay. *J. Neurosci.* **17,** 1880–1890 (1997).
17. Siapas, A. G., Lubenov, E. V. & Wilson, M. A. Prefrontal phase locking to hippocampal theta oscillations. *Neuron* **46,** 141–151 (2005).
18. Buzsáki, G. *et al.* Hippocampal network patterns of activity in the mouse. *Neuroscience* **116,** 201–211 (2003).
19. Kates, W. R. *et al.* The neural correlates of non-spatial working memory in velocardiofacial syndrome (22q11.2 deletion syndrome). *Neuropsychologia* **45,** 2863–2873 (2007).
20. Sobin, C. *et al.* Neuropsychological characteristics of children with the 22q11 deletion syndrome: a descriptive analysis. *Child Neuropsychol.* **11,** 39–53 (2005).
21. Lewandowski, K. E., Shashi, V., Berry, P. M. & Kwapil, T. R. Schizophrenic-like neurocognitive deficits in children and adolescents with 22q11 deletion syndrome. *Am. J. Med. Genet. B* **144B,** 27–36 (2007).
22. Bertolino, A. *et al.* Prefrontal-hippocampal coupling during memory processing is modulated by COMT Val158Met genotype. *Biol. Psychiatry* **60,** 1250–1258 (2006).
23. Esslinger, C. *et al.* Neural mechanisms of a genome-wide supported psychosis variant. *Science* **324,** 605 (2009).
24. Liu, H. *et al.* Genetic variation in the 22q11 locus and susceptibility to schizophrenia. *Proc. Natl Acad. Sci. USA* **99,** 16859–16864 (2002).
25. Mukai, J. *et al.* Evidence that the gene encoding ZDHHC8 contributes to the risk of schizophrenia. *Nature Genet.* **36,** 725–731 (2004).
26. Paterlini, M. *et al.* Transcriptional and behavioral interaction between 22q11.2 orthologs modulates schizophrenia-related phenotypes in mice. *Nature Neurosci.* **8,** 1586–1594 (2005).
27. Raux, G. *et al.* Involvement of hyperprolinemia in cognitive and psychiatric features of the 22q11 deletion syndrome. *Hum. Mol. Genet.* **16,** 83–91 (2007).
28. Yavich, L., Forsberg, M. M., Karayiorgou, M., Gogos, J. A. & Mannisto, P. T. Site-specific role of catechol-*O*-methyltransferase in dopamine overflow within prefrontal cortex and dorsal striatum. *J. Neurosci.* **27,** 10196–10209 (2007).

Supplementary Information is linked to the online version of the paper at www.nature.com/nature.

Acknowledgements We would like to thank M. Topiwala, A. Adhikari and Y. Sun for technical assistance. We also thank A. Adhikari, L. Drew and A. Arguello for comments on the manuscript. This work was supported by the Simons Foundation (J. A. Gogos), US National Institute of Mental Health grants MH67068 (M.K. and J. A. Gogos) and MH081968 (J. A. Gordon), and the Lieber Center for Schizophrenia Research and Treatment.

Author Contributions T.S., M.K., J. A. Gogos and J. A. Gordon designed the experiments. T.S. carried out the behavioural and electrophysiology experiments. K.L.S. engineered and supplied the mutant and control mice and contributed to the experimental design. T.S. and J. A. Gordon analysed the data. T.S., M.K., J. A. Gogos and J. A. Gordon interpreted the results and wrote the paper.

Author Information Reprints and permissions information is available at www.nature.com/reprints. The authors declare no competing financial interests. Correspondence and requests for materials should be addressed to J. A. Gordon (jg343@columbia.edu) or J. A. Gogos (jag90@columbia.edu).

©2010 Macmillan Publishers Limited. All rights reserved

METHODS

Surgery. Animals were initially anaesthetized with ketamine/xylazine, placed in a stereotaxic frame and maintained on isoflurane for the duration of the surgery. Craniotomies were made to allow two tetrodes or five stereotrodes to be implanted in the medial prefrontal cortex (mPFC; 1.7 mm anterior to the bregma, 0.4 mm lateral to the midline and 1.5 mm below the brain surface) and tungsten wires to be placed into the dorsal CA1 region of the hippocampus (1.94 mm posterior to the bregma, 1.5 mm lateral to the midline and 1.4 mm below the brain surface). Skull screws overlying the cerebellum and frontal cortex served as ground and reference, respectively. All wires were connected to a 16-channel interface and the mPFC electrodes were anchored to a microdrive that made it possible to advance them along the dorsoventral axis. To verify recording locations, current (50 μA, 10 s) was passed through the electrodes at the end of the experiment. Animals were then perfused, the brains cut on a cryostat and stained for Nissl bodies using cresyl violet. Representative lesions, as well as diagrams of recording locations, are shown in Supplementary Fig. 7. Nine wild-type mice were used for the experiment shown in Fig. 1. Nine *Df(16)A*$^{+/-}$ mice and ten of their wild-type littermates were used for the experiments involving genotype comparisons shown in Figs 2–4.

Behaviour. Animals were trained on a discrete non-match-to-sample spatial working memory task in a T-maze. Each trial of the task consisted of two phases. In the sample phase, mice ran down the centre arm of the maze and were directed into one of the goal arms. After a brief delay (~10 s) the mice again ran down the centre arm, but now had to choose between two open goal arms (choice phase). To obtain a reward, animals were required to enter the goal arm not visited during the sample phase. After two days of habituation to the maze and two days of shaping, animals were given daily training sessions of ten trials until they reached criterion performance, defined as performance of at least seven trials correct per day for three consecutive days. After this criterion had been reached, animals were given daily sessions of 20–25 trials. Although neural data was recorded throughout the experiment, the results presented here, with the exception of Fig. 3 and Supplementary Figs 4 and 5, are from these post-criterion sessions. mPFC electrodes were advanced regularly to ensure that different populations of cells were recorded in each behavioural session.

Phase-locking analysis. We examined synchrony within and across structures by asking whether the firing of prefrontal neurons was modulated by, or phase-locked to, the phase of ongoing field potential oscillations. We first filtered the field potentials in the theta range (4–12 Hz) using a zero-phase-delay filter (filter0, provided by K. Harris and G. Buzsaki) implemented in MATLAB (version 7.6, MathWorks). The filter uses a linear phase function (fir1; MATLAB Signal Processing Toolbox (version 6.9), MathWorks) and compensates for the phase delay by time-shifting the filtered signal. The phase of each sample of the filtered field potential was then computed using the Hilbert transform and each spike was then assigned the phase of its contemporaneous field potential sample. Phase-locking was quantified as the circular concentration of the resulting phase distribution, which we defined as the mean resultant length (MRL) of the phase angles. The MRL is the sum of the unit vectors representing the phases at which each spike occured, divided by the number of spikes. It therefore takes values between zero (no phase-locking) and one (perfect phase-locking). Previous studies[7,17] have used κ, the concentration parameter of the von Mises distribution, to quantify phase-locking. However, using κ instead of MRL yielded essentially identical results in our study; we chose MRL because it is the more intuitive metric of the two. The statistical significance of phase-locking was assessed using the Rayleigh test for circular uniformity.

To examine whether phase-locking was stronger to past phases of the theta oscillation or to future phases, we computed the MRL based on the phases at a fixed lag from each spike (range, −158–158 ms; step size, 26 ms). Of the lags at which phase-locking was significant (corrected for multiple comparisons), the one showing the highest MRL was defined as a neuron's 'preferred' lag. A neuron's preferred phase was then defined as the mean phase of its spike phase distribution at the preferred lag.

Sample estimates of MRL suffer from a positive bias (that is, they overestimate the population MRL) that is highly dependent on sample size. We therefore adopted two measures to limit the effects of this bias on our analysis. First, we only computed phase-locking for cells firing a minimum number of spikes. When comparing phase-locking in sample and choice phases, we considered only cells that fired at least 50 spikes under both conditions. When comparing phase-locking between genotypes, only cells firing at least 500 spikes during the entire session were included. Second, we made sure that the number of spikes did not differ across the conditions we sought to compare. When comparing phase-locking between sample and choice epochs within each cell, we subsampled the spikes from the task phase with more spikes so that equal numbers of spikes were used for calculating MRL. For comparisons across genotypes, the phase-locking of each cell was calculated from subsamples of 500 spikes. In both cases, subsamples were drawn repeatedly (1,000 times) and MRL values were first computed for each subsample and then averaged to yield the MRL estimate.

Asymmetry in the theta oscillation waveform can also give rise to spurious phase-locking, as more spikes will occur during the longer half of the cycle. To ensure that such asymmetry did not affect the results reported here, we performed two additional analyses. First, in addition to the Rayleigh test for circular uniformity, we calculated significance using a shuffling procedure to control for theta waveform asymmetries. For each cell, we shifted the theta-filtered field potential 5–10 s forwards or backwards in time and computed the phase of each spike relative to the shifted field potential and the MRL of the spike phase distribution. This was repeated 1,000 times for each cell, resulting in a distribution of MRL values that would be expected if mPFC neurons fired randomly with respect to (possibly asymmetric) theta oscillations. A cell was deemed significantly phase-locked if its measured MRL value was higher than the 95th percentile of the shuffling distribution. This yielded the same percentage of significantly phase-locked cells as in our initial analysis (66%). In addition, to ensure that differences in theta waveform asymmetry between the *Df(16)A*$^{+/-}$ and wild-type mice did not explain the differences in phase-locking, we demonstrated that theta asymmetry, as assayed by measuring the circular concentration of theta phase values, did not differ by genotype (Supplementary Fig. 6e).

To ensure that phase-locking strength was not affected by differences in the quality of cluster isolation, we performed several additional analyses. First, we computed for each cluster its isolation distance and L_{ratio} (ref. 29) as well as the signal-to-noise ratio[30]. Isolation distance and L_{ratio} were computed using 12 spike waveform features. For tetrodes, the features were energy and the first two principal-component coefficients; for stereotrodes, we used energy, peak, valley and the first three principal-component coefficients. There were no differences in any of the measures of cluster quality by genotype (Supplementary Fig. 2b). Second, we looked for correlations between phase-locking and isolation distance, both for the entire sample and for the subsample with isolation distance less than 20. No significant correlations were observed. Finally, the results presented here did not differ when we restricted our analysis to cells with isolation distance greater than 20, which constitute 81% of the units in the original sample.

Field potential analysis. Both the power spectral density and the coherence of field potentials were computed using the multi-taper method (MATLAB routines provided by K. Harris and G. Buzsaki). In outline, field potentials were divided into 800-ms segments (400-ms overlap) and the Fourier transform of each segment was computed after being multiplied by two orthogonal data tapers. Power spectral density was computed by averaging the power spectral densities across data windows and tapers. Coherence was computed by averaging the cross-spectral densities of two field potential signals across data windows and tapers and normalizing to the power spectral densities of each signal. Theta coherence was computed as the mean coherence in the 4–12-Hz range.

To measure the modulation of hippocampal gamma power by hippocampal theta phase, the hippocampal field potential was filtered for theta (4–12-Hz) and gamma (30–80-Hz) frequencies as described above. The instantaneous theta phase and gamma power were extracted using the Hilbert transform. The data were then divided into theta-phase bins and the mean gamma power was computed for each bin. The modulation index was defined as the difference between the highest and lowest gamma power across phase bins, divided by the highest power (that is, normalized modulation depth). To measure the correlation between pre-training theta coherence and learning rate, coherence was computed from neural activity recorded during a habituation session before the first training session. Only periods of continuous movement (speed $>10\,cm\,s^{-1}$) were used to get reliable estimates of theta coherence. To verify that the correlation was not simply due to the two genotypes differing in coherence and learning rate, we performed an analysis of covariance using genotype and coherence as independent variables and learning rate as the dependent variable.

29. Schmitzer-Torbert, N., Jackson, J., Henze, D., Harris, K. & Redish, A. D. Quantitative measures of cluster quality for use in extracellular recordings. *Neuroscience* **131**, 1–11 (2005).
30. Kelly, R. C. *et al.* Comparison of recordings from microelectrode arrays and single electrodes in the visual cortex. *J. Neurosci.* **27**, 261–264 (2007).

©2010 Macmillan Publishers Limited. All rights reserved